Dynamic scenarios of multistable switching in semiconductor superlattices

A. Amann,[1] A. Wacker,[1] L. L. Bonilla,[2] and E. Schöll[1,3]
[1]*Institut für Theoretische Physik, Technische Universität Berlin, Hardenbergstrasse 36, 10623 Berlin, Germany*
[2]*Escuela Politécnica Superior, Universidad Carlos III, Avenida de la Universidad 30, 28911 Leganés, Spain*
[3]*Department of Physics, Duke University, Durham, North Carolina 27708-0305*
(Received 19 December 2000; published 16 May 2001)

We analyze the dynamics of charge distributions in weakly coupled, doped, dc voltage biased semiconductor superlattices subject to voltage steps of different sizes. Qualitatively different current responses to voltage switching processes have been observed experimentally. We explain them by invoking distinct scenarios for electric-field domain formation, validated by numerical simulations. Furthermore, we investigate the transient from an unstable to a stable point in the current-voltage characteristics after a steplike or ramplike increase of the external voltage.

DOI: 10.1103/PhysRevE.63.066207 PACS number(s): 05.45.−a, 72.20.Ht

I. INTRODUCTION

Semiconductor superlattices (SL) typically exhibit ranges of negative differential conductivity that lead to self sustained current oscillations [1–4] due to traveling field domains, or a sawtoothlike multistable current-voltage (I-V) characteristic with many branches associated with static field domains [5–8]. Recently, the current response to switching from an initial voltage bias V_i to a final voltage V_f was investigated experimentally on the first plateau of a SL that exhibits multistable static field domains under dc voltage bias [9]. It was found that the dynamic response of the current changes dramatically when the voltage increase $V_{\rm step} = V_f - V_i$ surpasses a threshold value $V_{\rm crit}$.

In this paper, we analyze the dynamical evolution of the charge-density profile in a SL as the external voltage is either switched abruptly or ramped to a different value. Our study uses a microscopic model of sequential tunneling [10] to specify the current density in a set of discrete rate equations for electronic transport. Applying Ohmic boundary conditions, we find that different mechanisms of domain formation are effective. For small positive values of the switching voltage $V_{\rm step}$, the charge density located at the domain boundary moves upstream, *against* the direction of the charge transport, in order to form the new boundary. Meanwhile, the current relaxes monotonically to its new stationary value on the up-sweep branch. For larger positive values of $V_{\rm step}$, a downstream-moving charge dipole wave provides the mechanism for domain relocation, resulting in a nonmonotonic current response. Despite having *increased* the voltage, the system switches to a different operating point on the *down-sweep* branch of the I-V characteristic. For negative values of $V_{\rm step}$, the charge distributions always move in the direction of the field. By fitting one parameter in the boundary conditions, our model reproduces quantitatively the experimental results. Analysis of the boundary current is the key to understanding qualitatively why dipole waves appear, and to give criteria for monopole waves to occur. Furthermore, the size of the critical step voltage $V_{\rm crit}$ is qualitatively explained by using the relationship between the velocity of monopole waves and the total current [11].

We also study the transition from an unstable point of the current-voltage characteristic, P_u, to a stable point, P_s. In this process, the system remains in the immediate neighborhood of the unstable point during a time τ_d (the delay time) and then switches to the stable point P_s within a time τ_s (the switching time) [12]. For a given SL, we demonstrate that τ_s is almost constant. On the other hand, the delay time τ_d depends sensitively on the distance from P_u to the bifurcation point of the unstable branch and also on the ramping time needed to reach P_u. Again, the numerical results are in good agreement with the experimental data [9].

II. SEQUENTIAL TUNNELING MODEL

Oscillatory as well as static behavior in weakly coupled semiconductor SLs has been successfully described by a sequential tunneling model [13,14,4,10], where the electrons are assumed to be localized at the individual wells. For voltages within the first plateau of the SL I-V characeteristics, this model is justified in the regime where the lowest miniband width is smaller than the scattering width Γ. If the transversal relaxation is assumed to be fast compared to the longitudinal relaxation, there are no dynamical degrees of freedom in the transversal direction. For the transversal part of the electron wave function, we assume plane waves, specified by a two-dimensional wave vector $\mathbf{k}$. In the longitudinal z direction, we describe the localized electrons by one-dimensional Wannier functions $\Psi^{\mu}(z-md)$, where μ is the miniband index, m is the number of the well at which the Wannier function is localized, and d is the SL period [10]. Assuming local equilibrium within each well and constant broadening Γ^{μ} of the levels, the current density from well m to well $m+1$ is given by [10,15]

$$J_{m\to m+1}(F_m, n_m, n_{m+1}) = \sum_{\nu} \frac{e}{\hbar} |H^{1,\nu}_{m,m+1}|^2 \frac{\Gamma^1 + \Gamma^{\nu}}{(E^{\nu} - E^1 - eF_m d)^2 + \left(\frac{\Gamma^1 + \Gamma^{\nu}}{2}\right)^2} \times \{n_m - \rho_0 k_B T \ln[(e^{n_{m+1}/\rho_0 k_B T} - 1) e^{-eF_m d/k_B T} + 1]\}, \quad (1)$$

where $e<0$ is the charge of the electron, n_m is the two-dimensional electron density in well m, F_m is the electric field between the wells m and $m+1$ directed towards increasing m, E^ν is the energy level of the miniband ν, T is the temperature, $\rho_0 = m^*/\hbar^2\pi$ is the two-dimensional electron density of states, and m^* is the effective electron mass. The matrix elements $H^{1,\nu}_{m,m+1}$ between the Wannier states 1 in well m and ν in well $m+1$ are calculated numerically for a given SL from the Wannier functions [10].

The dynamic evolution of the electron densities is determined by the continuity equation

$$e\frac{dn_m}{dt} = J_{m-1\to m} - J_{m\to m+1} \quad \text{for} \quad m=1,\ldots,N. \tag{2}$$

The electron densities and the electric fields are coupled by the following discrete Poisson equation:

$$\epsilon_r\epsilon_0(F_m - F_{m-1}) = e(n_m - N_D) \quad \text{for} \quad m=1,\ldots,N, \tag{3}$$

where N_D is the two-dimensional doping concentration, N is the number of wells in the SL, F_0 and F_N are the fields at the emitter and collector barrier, and ϵ_r and ϵ_0 are the relative and absolute permittivities. In order to derive Eq. (3), we consider Gauss's law in the integral formulation, with the integration volume being a well, modeled by an infinite layer with finite width w. Then Eq. (3) follows under the conditions that the charge is localized within the wells, and the charge distribution does not depend on the transversal coordinates. These conditions are fulfilled, since the electron wave functions are assumed to be Wannier functions in the longitudinal direction and plane waves in the transversal direction, and the background charge due to doping is assumed to be confined to the center of the well. By differentiating Eq. (3) with respect to time and using Eq. (2), we obtain the following equation for the field F_m:

$$\epsilon_r\epsilon_0\frac{dF_m}{dt} + J_{m\to m+1} = J \quad \text{for} \quad m=1,\ldots,N, \tag{4}$$

where J is the total current density, independent of the well index. The total voltage drop U between emitter and collector provides a global coupling by

$$U = \sum_{m=0}^{N} F_m d. \tag{5}$$

Notice that for high fields (such as those in higher plateaus of the *I-V* characteristic), the last factor in the tunneling current (1) becomes n_m. Then the system (3)–(5) reduces to the well-known discrete drift model of Refs. [4] and [14].

Under dc voltage conditions, it is known that the choice of the boundary current crucially influences the dynamical behavior [16]. In particular, self-sustained oscillations of the current may be due to recycling and motion of either monopole or dipole charge waves: boundary conditions resulting in charge accumulation (or depletion) at the emitter contact favor monopole wave dynamics [16]. If the boundary conditions can result both in charge depletion and accumulation, dipole charge waves can be injected. In principle, it is possible to derive idealized boundary currents at the contact regions by a microscopic approach based on the transfer Hamiltonian method [17–19]. Real contact regions consist of a number of layers differing in composition and doping. Given the real configuration of a contact region, the value that should be assigned to the contact doping in the idealized microscopic model is not completely clear [17–19]. We have chosen not to model the contact layers, for this would noticeably complicate our analysis. Thus we have preferred a different approach. Instead of using specific boundary currents coming from microscopic contact modeling, we have selected the following simple Ohmic boundary currents in this paper:

$$J_{0\to 1} = \sigma F_0, \tag{6}$$

$$J_{N\to N+1} = \sigma F_N \frac{n_N}{N_D}, \tag{7}$$

where σ is the Ohmic conductivity, and the factor n_N/N_D is introduced in order to avoid negative electron densities at the collector [20]. More realistic nonlinear boundary currents will provide the same qualitative dynamical behavior as the previous Ohmic currents with appropriately chosen σ, depending on the contact doping [19]. In Sec. V, we discuss the implications of choosing different values for σ in more detail. The experimental observations in Ref. [9] (Fig. 5) and Ref. [21] (Fig. 3) show that the current response after a large increase of the external voltage exhibits a typical troughlike structure with an almost flat minimum. This indicates that for these superlattices, dipole waves provide the mechanism for the switching process. The reason is that a dipole wave detached from the contacts moves at a roughly constant speed corresponding to a roughly constant current. We therefore select σ such that dipole waves are triggered at the emitter contact. As we will show in Sec. V, boundary conditions that trigger monopole waves result in a continuously changing current, since monopole waves change speed. This behavior is well known in the limiting case of a very large SL (continuum limit [22], corresponding to the Gunn effect in bulk GaAs [23,24]).

III. NUMERICAL SIMULATION

We simulate numerically an $N=40$-well SL with barrier width $b=4.0$ nm, well width $w=9.0$ nm, doping $N_D=1.5\times10^{11}$ cm^{-2}, $\Gamma=8$ meV (independent of the miniband index μ), and cross section $A=15\,000$ μm^2, at a temperature $T=5$ K. The parameters are those of the SL in Ref. [9]. Reasonable agreement with the overall shape of the experimental current-voltage characteristics in Ref. [9] is found if we adopt $\sigma=0.01$ $(\Omega\,\mathrm{m})^{-1}$.

For the homogeneous case, i.e., $n_m=n_{m+1}$, the current density (1) depends on the electric field as in Fig. 1, yielding a typical *N*-shaped curve. The corresponding stationary current-voltage characteristics for inhomogeneous solutions is the typical sawtooth pattern of Fig. 2 with upper and lower

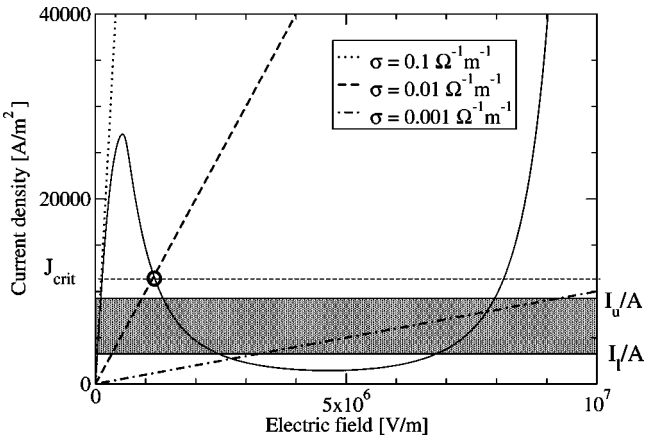

FIG. 1. Current density vs electric-field characteristic between two neutral wells (solid curve) and at the emitter barrier for Ohmic boundary currents, with various conductivities σ (dashed). The shaded area marks the regime of stationary fronts.

branches corresponding to up- and down-sweep of the external voltage, respectively.

It is important to note that the system of ordinary differential equations (2)–(5) is stiff [25], since

$$\left|\frac{J_{m-1\to m}-J_{m\to m+1}}{J_{m-1\to m}+J_{m\to m+1}}\right| \ll 1. \tag{8}$$

Therefore, implicit integration methods are necessary to obtain stable solutions. In our case, we used a fifth-order implicit Runge-Kutta solver and verified the results using a standard backward differentiation formula (BDF) solver [26].

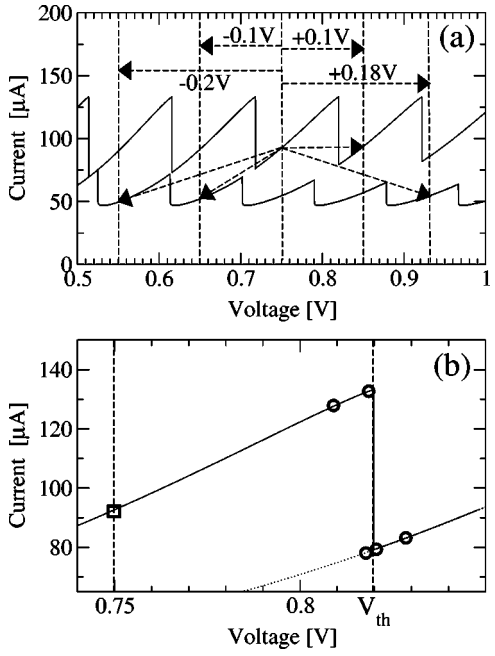

FIG. 2. Simulated sawtooth current-voltage characteristic of a 40-well superlattice (4.0 nm AlAs barriers, 9.0 nm GaAs wells). Upper branches correspond to voltage up-sweep, lower branches to down-sweep. The arrows in (a) indicate the starting and end points of the voltage steps discussed in Sec. IV. (b) gives an enlarged view of the initial operating point (box) as well as of the different final points (circles) considered in Sec. VI.

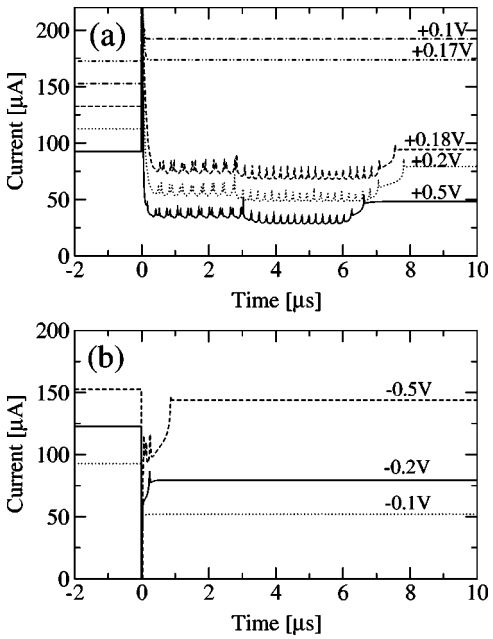

FIG. 3. Current response vs time for various (a) positive and (b) negative voltage steps at $t=0$. For $t<0$, the voltage is $V_i=0.75$ V. The curves are shifted vertically in units of 20 μA in (a) and 30 μA in (b) for clarity.

We shall investigate here the SL response to switching or ramping starting from a point on the upper branch of the first plateau of the *I-V* characteristic at $V_{dc}=0.75V$ (Fig. 2). After switching to a final voltage $V_f=V_{dc}+V_{step}$, the current will evolve towards a value on the stationary *I-V* characteristic corresponding to one of the branches at voltage V_f (in general there are several such branches due to multistability).

We find that the final stationary current is on the upper branch if $V_{step}=0.1$ V, while it is on the lower branch if $V_{step}=0.18$ V; see the arrows in Fig. 2(a). Thus fast switching allows us to reach the lower branch by just increasing the voltage sufficiently. This is a striking result: In conventional up- and down-sweep, the point on the lower branch at 0.93 V can only be reached by increasing the voltage to more than 1.1 V and then decreasing to 0.93 V.

In Fig. 3(a), we depict the current response to different positive values of V_{step} versus time. For

$$V_{step} < V_{crit}, \tag{9}$$

with $V_{crit}\approx 0.175$ V, the current relaxes monotonically to its final value. There is a fundamentally different current response if Eq. (9) does not hold. Instead of relaxing monotonically, the current first drops to a level well below the lower stationary branch. Then the current response exhibits a fast repetitive double-peak pattern until about 3 μs. Subsequently, following one larger spike, only single peaks occur. The spiky structure ends about 7 μs after the voltage switch, and the current evolves to a stationary value on the lower branch. The total number of peaks is roughly equal to the

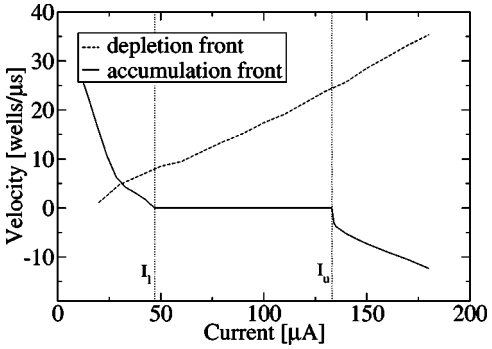

FIG. 4. Front velocity vs current for electron depletion and accumulation fronts.

number of wells in the SL. The frequency of the peak burst is about 15 MHz. This behavior does not change significantly as long as Eq. (9) is violated, even for very different values of V_{step}. This effect is very similar to the experimental observations in Ref. [9]. The quantitative difference is that the experimental total relaxation time is only about 2 μs. Such values could be achieved numerically, by choosing a larger scattering width $\Gamma \approx 20$ meV. The current response of the SL in Ref. [21] exhibits a total relaxation time of about 6 μs for the second plateau, and its current response during the switching process shows a peaklike structure very similar to our numerical results.

IV. SWITCHING MECHANISM

We now explain the reason for this behavior qualitatively. For this purpose, it is very helpful first to consider the velocities of electron accumulation and depletion fronts as a function of the current, as depicted in Fig. 4 (see also Ref. [11]). Notice that electron accumulation monopoles may have positive, zero, or negative velocities as the current is increased. The current interval (I_l, I_u) corresponding to stationary monopoles depends on the location and size of the peak and bottom values of the sequential tunneling current Eq. (1). For a current below this interval, the charge monopole moves downstream towards the collector, whereas for a current above this region, it moves upstream towards the emitter, against the direction of the electron motion [11]. At the boundaries of the static front regime, the front velocity scales as $v \sim \sqrt{|I - I_{u/l}|}$. This scaling behavior is also found for pinned waves in diffusion systems with discrete sources [27]. The backward motion of the monopole occurs only for voltages on the first plateau of the *I-V* characteristic, where the tunneling current Eq. (1) depends appreciably on n_{m+1} [11].

It is also evident from Fig. 4 that electron depletion waves always have positive velocity, which means that they move towards the collector. Their velocity increases approximately linearly with increasing current (Fig. 4). For depletion waves, $n_m \ll N_D$ and $F_m - F_{m-1} \approx -eN_D/(\epsilon_r \epsilon_0)$, we can ignore the tunneling current $J_{m \to m+1}$ in Eq. (4), and therefore the front velocity is approximately $J/(eN_D)$ [22,24]. The point in Fig. 4 where the velocities of accumulation and depletion fronts intersect is of special interest: This point determines the velocity and current at which a dipole wave consisting of a leading depletion front and a trailing accumulation front can move rigidly [24].

Let us now consider a switching process where condition (9) is fulfilled and $V_{\mathrm{step}} > 0$. From the dynamical evolution of the electron densities n_i, which is depicted in Fig. 5(a) for $V_{\mathrm{step}} = 0.1$ V, we observe that the charge monopole region of high electron density (light region) is shifted upstream (against the field eF) towards the emitter. This shifting occurs on a time scale of 0.1 μs, explaining the fast monotonic relaxation if Eq. (9) is fulfilled. The switching to a higher external voltage has the effect that all fields in the superlattice are increased and the current instantaneously rises above I_u. According to Fig. 4, this gives rise to a negative velocity of the accumulation front.

If condition (9) is violated, the switching scenario is more complicated. For $V_{\mathrm{step}} = 0.18$ V and $V_{\mathrm{step}} = 0.50$ V, the evolution of the electron density profile is depicted in Figs. 5(b) and 5(c), respectively. Before switching V_{step}, there is a

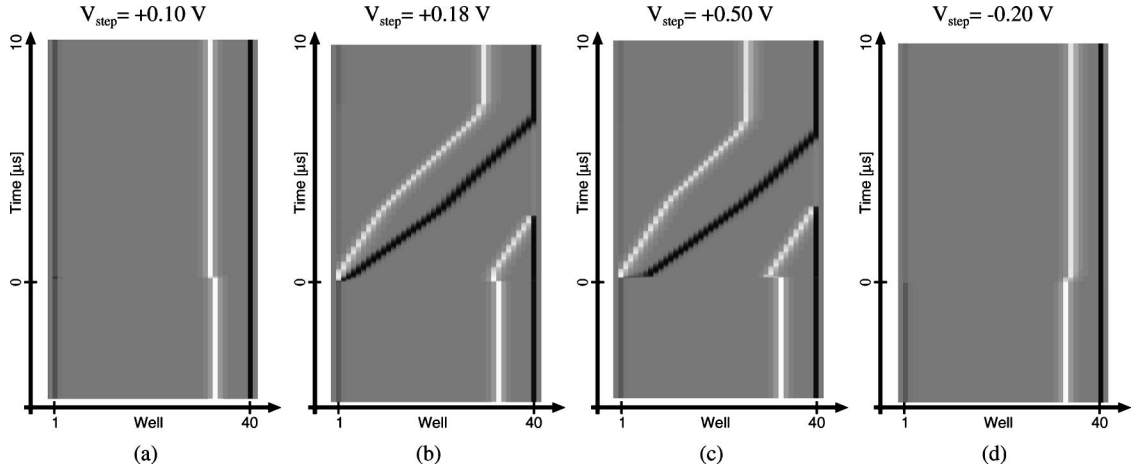

FIG. 5. Evolution of electron densities in the quantum wells during the switching process for various voltage steps. White indicates high electron density (accumulation front), black indicates low electron density (depletion front). In the gray area, the electron density is $\approx N_D$. Well no. 1 is located at the emitter, well no. $N = 40$ at the collector. At $t = 0$, a voltage step V_{step} is applied, starting from $V_i = 0.75$.

charge accumulation front inside the sample corresponding to the domain wall separating two coexisting stationary high-field domains. After switching the voltage, the charge dynamics in the superlattice exhibits three different phases: (i) upstream shift of the accumulation front and generation of new fronts at the emitter, (ii) coexistence of three fronts in downstream motion, and (iii) downstream motion of two fronts. These three phases will now be considered in detail.

Phase (i). Shortly after switching the voltage step, the original preexisting electron accumulation layer moves upstream towards the emitter. Simultaneously, a charge dipole wave appears at the emitter. Its leading depletion front moves towards the collector while its amplitude increases. The trailing electron accumulation front of the dipole is pinned at the first SL well.

The mechanism for the generation of a dipole at the emitter is as follows: In a stationary situation, the current through the emitter barrier is equal to the current through the first SL barrier. The field at the emitter can be calculated from Fig. 1, where the boundary current at the emitter is compared to the homogeneous current-field characteristic. Notice that both currents intersect on the second branch of the homogeneous current-field characteristic, at a critical value J_{crit}, because we have chosen the slope of the emitter current to be lower than the slope of the homogeneous low-field current-field characteristic. If $0<J<J_{\mathrm{crit}}$, the field at the emitter barrier is larger than that at the first barrier, $F_0>F_1$. Then the Poisson equation predicts electron depletion, $n_1<N_D$. If we could suddenly change the current to a value larger than J_{crit}, the field F_1 would increase according to Eq. (4), trying to attain a value on the third branch of the characteristic curve of Fig. 1. This would produce an electron accumulation layer at this well followed by the depletion layer that was there before changing J. The net outcome of this mechanism would be the creation of a dipole. As seen in Fig. 4, a depletion layer separated from the contacts has to move towards the collector, at a speed proportional to J. As it moves, it leaves a high-field region behind. The increase of length gained by this region has to be compensated by lowering the current (for both the low-field and the high-field domains occur in a region of positive differential conductivity) so as to keep the total voltage constant.

Phase (ii). After about 0.2 μs, the current has dropped below I_l, which from Fig. 4 means that all fronts have positive velocities. The original accumulation layer and the trailing accumulation front start advancing towards the collector with the same velocity, while the positively charged leading front of the dipole moves towards the collector at a higher velocity. What is this velocity? First of all, notice that the mean value of the current is approximately constant during the transients that follow the voltage step in Fig. 3(a). Shifting by one well towards the collector, the depletion front diminishes the high-field domain and expands the low-field domain by one well, while shifting of any accumulation front has the contrary effect. Since the external bias is fixed, a quasisteady situation results only if the sum of the velocities of the two accumulation fronts is equal to the velocity of the depletion front. Then the current takes on a constant mean value corresponding to $2\,c_+(I)=c_-(I)$, where $c_\pm(I)$ are the velocities of the positively or negatively charged fronts depicted in Fig. 4. Each time an accumulation layer advances by a SL period, a spike of the current appears, which explains the double-peak structure observed in the numerical simulation of Fig. 3(a). Notice that the transient region where the current exhibits double spikes has a flat appearance, indicating a constant *mean value* of the current.

Phase (iii). After the original accumulation layer has reached the collector at $t_o\approx 3$ μs, there are only one accumulation layer and one depletion layer present in the sample, giving rise to a single-spike structure of the current response as depicted in Fig. 3(a). By the same reasoning as in (ii), the velocities of the positively and negatively charged fronts are now required to fulfill the condition $c_+(I)=c_-(I)$. The current is then fixed to the crossing point of the two front velocities as depicted in Fig. 4. In comparison to phase (ii), the velocity of the accumulation front has almost doubled, while the velocity of the depletion front has decreased slightly.

After these three stages of its evolution, the accumulation front finally reaches a stable stationary state: it becomes the domain wall separating two stationary high-field domains. Of all such possible stationary solutions at voltage $V_{\mathrm{dc}}+V_{\mathrm{step}}$, the one having an accumulation layer closer to the emitter is reached. This final situation on a low current branch of the current-voltage characteristics at voltage $V_{\mathrm{dc}}+V_{\mathrm{step}}$ could also be reached by conventional down-sweeping the current-voltage characteristics. In the latter case, the electron accumulation layer also moves towards the collector.

For $V_{\mathrm{step}}<0$, the electron accumulation layer always travels towards the collector and stops at a position corresponding to the domain wall separating low- and high-field domains of a stationary solution. This solution is the same as what could be reached by down-sweeping to the final voltage, Fig. 5(d). Contrary to the case of positive V_{step}, the resulting current response shows no thresholdlike behavior; see Fig. 3(b). Since all fields decrease during the switching process, no dipole wave can be generated at the emitter.

V. BEHAVIOR FOR A DIFFERENT BOUNDARY CONDITION

The dipole domain formation mechanism is different from the monopole mechanism described in Ref. [28]. The selection mechanism for dipole or monopole wave generation at the emitter depends on the boundary condition there [23]. If the boundary condition allows both electron accumulation and depletion at the emitter, a dipole wave can be created. If the boundary condition allows only electron accumulation, only monopole waves can arise at the emitter.

As discussed above, the mechanism of current response to a voltage switch involving dipole domains depends decisively on the emitter differential conductivity being lower than that of the homogeneous current-field characteristic. In Fig. 6(a), the current response for $\sigma=0.1\ (\mathrm{m}\,\Omega)^{-1}$ is depicted. We observe that the current response exhibits a U-shape behavior for large V_{step}. Figure 6(c) shows that the domain formation mechanism is now mediated by well-to-well hopping of charge monopoles, as was the case discussed

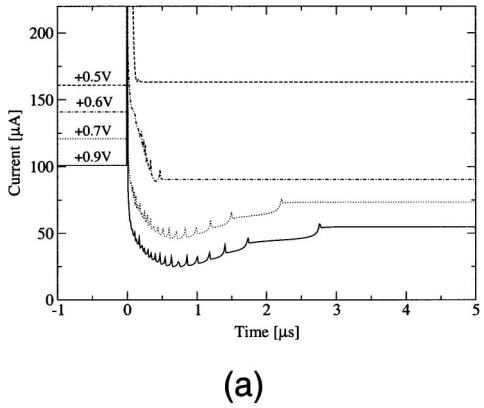

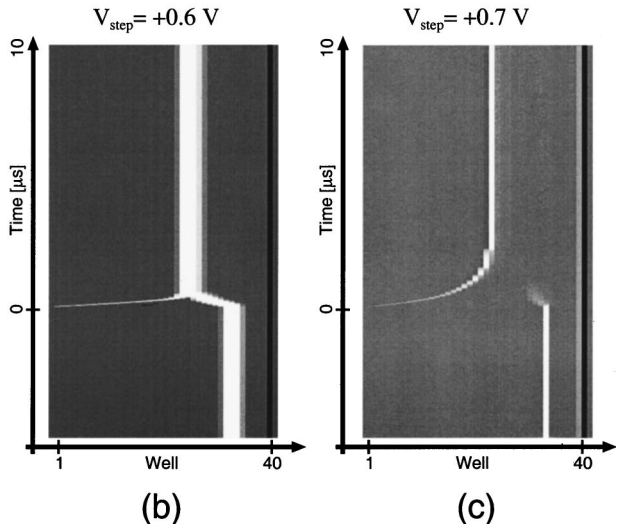

FIG. 6. Current response (a) and evolution of electron densities (b),(c) for $\sigma = 0.1\ (\Omega\ \mathrm{m})^{-1}$. Note that in (b) and (c), different gray scales are used.

in Ref. [28]. If only monopoles are present in the SL, their motion can be compatible with the dc bias condition only if the current (and therefore the monopole velocity) changes continuously [22]. This also implies that the overall time for stable domain formation depends on V_{step}.

The mechanisms of monopole domain formation at the emitter and domain boundary relocation may coexist, as indicated by Fig. 6(b). Here two monopole accumulation fronts move in opposite directions inside the SL. This seems to contradict the observation that the front velocity is a unique function of the current, as depicted in Fig. 4. However, Fig. 4 corresponds to velocities of fully developed monopoles, whose domain walls join a low- and a high-field domain in a quasisteady situation. The front coming from the emitter in Fig. 6(b) joins a low-field domain to a transient domain at an intermediate field [22]. Thus it is not a fully developed monopole, and its velocity is different from that of the front making up the original domain boundary. The coexistence of those two domain formation mechanisms results in a smoother transition from the boundary relocation mechanism to the monopole domain formation mechanism with increasing V_{step}. This contrasts with the situation in the dipole regime discussed before: there, both types of domain formation

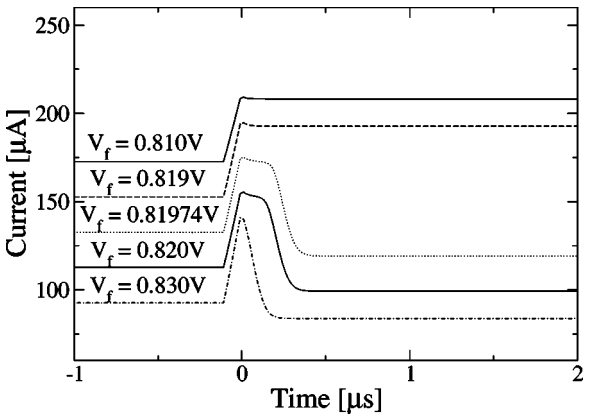

FIG. 7. Current response for sweeping the voltage from $V_i = 0.75$ V to various final voltages V_f [cf. circles in Fig. 2(b)]. We use a constant ramp time of $\tau_r = 100$ ns. The curves are shifted vertically in units of 20 μA for clarity.

mechanisms do not coexist, and therefore a sharper transition between the two mechanisms occurs: compare Figs. 3(a) and 6(a).

Finally, if σ is chosen to be so small that J_{crit} is below I_l/A, which is the critical value for static fronts under current bias, dipole waves are generated under constant voltage conditions. This leads to oscillating behavior akin to the Gunn effect [10,23].

VI. TRANSITION FROM UNSTABLE TO STABLE POINTS

In Ref. [9], the current response to a switching process, where the final voltage V_f is close to a discontinuity in the current-voltage characteristic, was measured. In contrast with the results discussed above, V_{step} is now typically less than 0.1 V [see Fig. 2(b)], and the dipole domain formation mechanism cannot occur. It was found experimentally that the transition time is less than 0.1 μs, provided that the final point, $P_f = (V_f, I_f)$, is on the same branch of the current-voltage characteristic as the initial point, $P_i = (U_i, I_i)$. If P_f and P_i are on different branches, then the transition time increases if the distance from V_f to the threshold voltage V_{th} decreases. This behavior can be reproduced by our model, as is shown in Fig. 7(a). Here the branch discontinuity is located at $V_{\mathrm{th}} = 0.819\,72$ V, and the transition time increases as the distance from V_f to V_{th} decreases.

A theoretical explanation of this behavior is as follows. Let us again consider the relationship between monopole front velocity and current. If initial and final voltages are on the same branch of the current-voltage characteristic, the current responds to the voltage switch by a small continuous increase. The SL charge profile has a peak that is still located at the same well as before the switch, but its center of mass has shifted slightly towards the emitter. Suppose now that the final voltage is located beyond the threshold in the current-voltage characteristic. Then the current first increases to a value beyond the end of the initial branch of the I-V characteristics, I_u, above which accumulation layer monopoles can move against the flow of electrons at constant current bias [11] (Fig. 4). The field and charge profiles first start changing without changing the location of the charge peak.

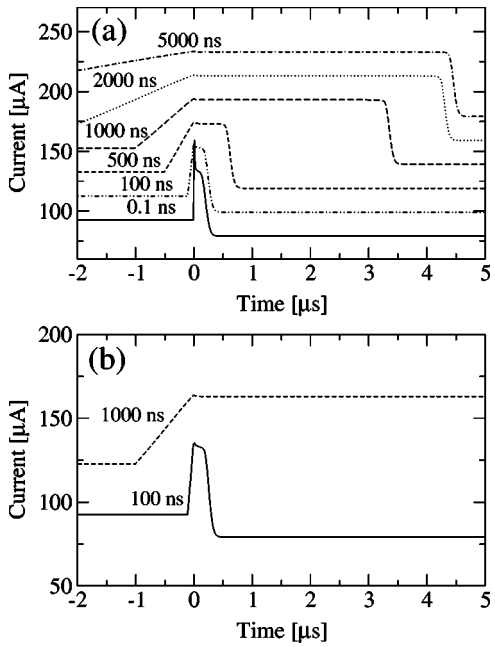

FIG. 8. Current response for sweeping the voltage from 0.75 V to (a) $V_f = 0.819\,74$ V, and (b) $V_f = 0.819\,70$ V during different ramp times. For the sake of clarity, the curves in (a) and (b) are shifted vertically in units of 20 μA and 30 μA, respectively.

During a time τ_d, they manage to shift the center of mass of the charge profile upstream without changing the location of its maximum, and keeping $I \approx I_u$. This situation is unstable because the center of mass and the charge peak cannot be separated too far. Thus the charge peak has to move upstream towards the emitter after a delay time τ_d. Then the current drops fast until the stationary configuration corresponding to the next branch in the current-voltage characteristic is reached. Let us denote by τ_s the switching time during which the current drops from I_u to its final stationary value I_f. A close look at Fig. 7 shows that the delay time τ_d (during which $I \approx I_u$) depends on the final voltage V_f, while the switching time τ_s does not.

The above discussion makes it clear that long delay times can be achieved if we manage to keep the current very close to I_u after changing the voltage to V_f. If the switching process is fast, the subsequent current peak is sharp: in this case, low- and high-field domains occur in a region of positive differential conductivity and the resulting situation is stable (and is reached exponentially fast). Longer delay times can be achieved by using a ramplike sweeping process to reach V_f instead of a fast step-switching process. In Fig. 8(a), we show the effect of using different sweeping times. Here the final bias V_f is reached at $t=0$. We observe that the delay time increases by a factor of 8 if we augment the ramp time, τ_r, from 100 ns to 1000 ns. Further increase of the ramp time has no significant effect, since the contribution of the peak current to the absolute current becomes neglible. On the other hand, if we sweep fast enough, we can achieve a transition to a different branch even if $V_f < V_{\rm th}$. This is shown in Fig. 8(b), where we can selectively reach two different points in the current-voltage characteristic, by changing the ramp time from 100 ns to 1000 ns. Note that this selection of multistable points is different from the selection due to different domain formation mechanisms, as discussed in Sec. IV.

VII. CONCLUSIONS

Provided that Ohmic boundary conditions are chosen to model the contact regions, we have shown that different mechanisms for domain formation occur for different boundary conditions and sizes of the voltage step in domain-wall relocation experiments. For negative or small positive values of $V_{\rm step}$, the charge accumulation layer separating two domains moves to its new location. For large positive values of $V_{\rm step}$, a dipole wave may provide the mechanism for domain-wall formation. In this case, the final operating point corresponds to a point on the down-sweep branch of the static current-voltage characteristics. One possible application of this feature could be a device that limits the current if the voltage increases linearly with time with a slope larger than a certain threshold value.

Two generic times characterize the transition from unstable to stable operating points on the current-voltage characteristic: a delay time and a switching time. During the delay time, the current is close to the maximum value on the current-voltage characteristics, whereas it drops down to its final stable value after the switching time. While the latter is essentially constant, the delay time depends very sensitively upon the ramp time, after which the unstable point is reached, and on the distance from the final voltage to the discontinuous threshold in the static current-voltage characteristics. If the final voltage corresponds to a stable point just below the threshold, switching to a different stable branch can nevertheless be caused by a fast voltage ramp.

ACKNOWLEDGMENTS

We thank A. Carpio, H. T. Grahn, P. Rodin, M. Rogozia, and S. W. Teitsworth for fruitful discussions. This work has been supported by DFG in the framework of Sfb 555, by the TMR Contract No. ERB FMBX-CT97-0157, and by the Spanish DGES through Grant No. PB98-0142-C04-01. E.S. thanks the Fulbright Foundation for financial support.

[1] M. Büttiker and H. Thomas, Phys. Rev. Lett. **38**, 78 (1977).

[2] J. Kastrup, R. Klann, H. T. Grahn, K. Ploog, L. L. Bonilla, J. Galán, M. Kindelan, M. Moscoso, and R. Merlin, Phys. Rev. B **52**, 13 761 (1995).

[3] K. Hofbeck, J. Grenzer, E. Schomburg, A. A. Ignatov, K. F. Renk, D. G. Pavel'ev, Y. Koschurinov, B. Melzer, S. Ivanov, S. Schaposchnikov, and P. S. Kop'ev, Phys. Lett. A **218**, 349 (1996).

[4] J. Kastrup, R. Hey, K. H. Ploog, H. T. Grahn, L. L. Bonilla, M. Kindelan, M. Moscoso, A. Wacker, and J. Galán, Phys. Rev. B **55**, 2476 (1997).
[5] L. Esaki and L. L. Chang, Phys. Rev. Lett. **33**, 495 (1974).
[6] Y. Kawamura, K. Wakita, H. Asahi, and K. Kurumada, Jpn. J. Appl. Phys., Part 2 **25**, L928 (1986).
[7] H. T. Grahn, R. J.. Haug, W. Müller, and K. Ploog, and G. H. Döhler, Phys. Rev. Lett. **67**, 1618 (1991).
[8] Y. A. Mityagin, V. N. Murzin, Y. A. Efimov, and G. K. Rasulova, Appl. Phys. Lett. **70**, 3008 (1997).
[9] K. J. Luo, H. T. Grahn, and K. H. Ploog, Phys. Rev. B **57**, 6838 (1998).
[10] A. Wacker, in *Theory of Transport Properties of Semiconductor Nanostructures*, edited by E. Schöll (Chapman and Hall, London, 1998), Chap. 10.
[11] A. Carpio, L. L. Bonilla, A. Wacker, and E. Schöll, Phys. Rev. E **61**, 4866 (2000).
[12] H. K. Charles, Jr. and C. Feldman, J. Appl. Phys. **46**, 819 (1975).
[13] F. Prengel, A. Wacker, and E. Schöll, Phys. Rev. B **50**, 1705 (1994); **52**, 11 518 (1995).
[14] L. L. Bonilla, J. Galán, J. A. Cuesta, F. C. Martínez, and J. M. Molera, Phys. Rev. B **50**, 8644 (1994).
[15] A. Wacker, Phys. Rep. (to be published).
[16] D. Sánchez, M. Moscoso, L. L. Bonilla, G. Platero, and R. Aguado, Phys. Rev. B **60**, 4489 (1999).
[17] V. J. Goldman, D. C. Tsui, and J. E. Cunningham, Phys. Rev. B **35**, 9387 (1987).
[18] R. Aguado, G. Platero, M. Moscoso, and L. L. Bonilla, Phys. Rev. B **55**, 16 053 (1997).
[19] L. L. Bonilla, G. Platero, and D. Sánchez, Phys. Rev. B **62**, 2786 (2000).
[20] H. Steuer, A. Wacker, and E. Schöll, Physica B **272**, 202 (1999).
[21] Y. Shimada and K. Hirakawa, Jpn. J. Appl. Phys., Part 1 **36**, 1944 (1997).
[22] L. L. Bonilla, M. Kindelan, M. Moscoso, and S. Venakides, SIAM (Soc. Ind. Appl. Math.) J. Appl. Math. **57**, 1588 (1997).
[23] F. J. Higuera and L. L. Bonilla, Physica D **57**, 161 (1992).
[24] L. L. Bonilla, I. R. Cantalapiedra, G. Gomila, and J. M. Rubí, Phys. Rev. E **56**, 1500 (1997).
[25] J. Stoer and R. Bulirsch, *Introduction to Numerical Analysis* (Springer-Verlag, New York, 1992).
[26] H. Olsson, The Godess Project, Software Library, Department of Computer Science, Lund, Sweden (1998).
[27] I. Mitkov, K. Kladko, and J. E. Pearson, Phys. Rev. Lett. **81**, 5453 (1998).
[28] J. Kastrup, F. Prengel, H. T. Grahn, K. Ploog, and E. Schöll, Phys. Rev. B **53**, 1502 (1996).